Journal of Molecular Spectroscopy 293–294 (2013) 27–32

Contents lists available at ScienceDirect

Journal of Molecular Spectroscopy

journal homepage: www.elsevier.com/locate/jms

Climbing up the vibrational ladder of $HC^{15}N$: High-temperature near-infrared emission measurements

A. Predoi-Cross [a,*], E. Johnson [a,1], D. Hemsing [a,1], H. Rozario [a], Georg Ch. Mellau [b]

[a] Alberta Terrestrial Imaging Centre, Department of Physics and Astronomy, University of Lethbridge, Lethbridge, AB T1K 3M4, Canada
[b] Physikalisch-Chemisches-Institut, Justus-Liebig-Universität Giessen, Heinrich-Buff-Ring 58, D-35392 Giessen, Germany

ARTICLE INFO

Article history:
Received 6 July 2013
In revised form 1 October 2013
Available online 21 October 2013

Keywords:
$HC^{15}N$
Molecular spectra
Infrared spectra
Emission spectra
Bending vibrations
Rovibrational constants

ABSTRACT

The near-infrared (NIR) emission spectrum of $H^{12}C^{15}N$ was measured in the 6050–6500 cm^{-1} range at a resolution of 0.044 cm^{-1} using an emission setup available at the Justus-Liebig Universität, Giessen, Germany. The rich emission spectrum showing numerous overlapped spectral profiles was analyzed with the spectrum analysis software SyMath running using Mathematica as a platform. This approach allowed us to retrieve the vibrational–rotational constants for 32 bands. Many spectroscopic transitions have been observed for the first time in a lab environment. We quantified four newly observed Coriolis resonances.

1. Introduction

Astrobiological processes within the Universe began with the synthesis of the fundamental elements that are required for life: hydrogen, carbon, oxygen, nitrogen, sulfur, and phosphorus. These base elements originate as derivatives of the stellar nucleosynthesis of heavy elements (a phenomenon which appears to be widespread within our Galaxy). Given favorable conditions, the transition of these elements to higher molecules and compounds becomes natural. The advancement, or evolution, of these compounds is of significant interest when particularly regarding their formulation into organic molecules.

Biological compounds such as amino acids and nucleic acids (DNA and RNA) are commonly accepted as the "building blocks" of life and their existence alone fosters the potential for the development of life. Contemporary theories postulate this possibility and consequently the prebiotic synthesis of amino and nucleic acid have been studied in the laboratory under planetary-like conditions. A similar environment to the one hypothesized to exist upon Jupiter's moon Europa has been modeled experimentally and the chemistry relevant to the formation of life has repeatedly been produced [1].

Hydrogen cyanide (HCN) is a key intermediary molecule for the synthesis of biochemical compounds and has received a lot of attention due to its astrophysical significance and prevalence [2]. Of its many potential sources, HCN may be formed through the decomposition of various cyanide compounds (such as CH_3CN or NH_4CN) by means of ionizing radiation and light in general [3,4].

The veracity of these postulated conditions and their consequent laboratory simulations were further substantiated in July of 1994 when comet Shoemaker-Levy 9 collided with Jupiter and its atmosphere. Observations made from both earth-based and space remote sensing instruments detected strong HCN lines (among those of other typically trace species) in the millimeter and submillimeter regions of the spectrum. After a 4 year surveillance of the planet's atmosphere it was decided that the compounds were indeed produced from the collision itself [5].

With the presence of hydrogen cyanide, several documented chemical reactions have been shown to generate a vast array of biochemical constituents. For example, in the synthesis of adenine (one of the four principle nucleic acids), HCN undergoes a self-condensation reaction to yield diaminomaleonitrile ($C_4H_4N_4$) which in turn combines with formamidine (CH_4N_2) to create the compound [6]. Furthermore, formamide – which interestingly is derived from HCN under certain conditions – has also been shown to generate adenine in other reactions [6]. On the same subject, the presence of HCN in its monomeric and/ or polymeric form within liquid water can lead to the formation of amino acids [1].

After discussing these situations, it should be noted that several considerations are yet to be resolved regarding the prebiotic

* Corresponding author. Fax: +1 403 329 2057.
E-mail address: Adriana.predoicross@uleth.ca (A. Predoi-Cross).
[1] Present address: Department of Physics, University of Alberta, 11322-89 Avenue, Edmonton, AB T6G 2G7, Canada.

0022-2852/$ - see front matter © 2013 Elsevier Inc. All rights reserved.
http://dx.doi.org/10.1016/j.jms.2013.10.002

formation of these compounds and particularly their relation to the current origin-of-life theories [7]. However, HCN does provide an attractive possibility to substantiate these developing theories. In addition to this, HCN has also become a reliable indicator of wounded, dying, or burning biomass emissions through the use of remote sensing and spectroscopy [8,9]. Significant increases of HCN were identified in localized areas during drought conditions in tropical Southeast Asia, the El Niño warm phases, and when large amounts of biomass burning took place [9].

The spectrum of $H^{12}C^{14}N$ and of the $H^{14}N^{12}C$ isotopologue have been studied extensively because of its relative simplicity and yet its ability to show many features that are of interest from a fundamental, theoretical point of view. Especially, the bending vibration is of particular interest to us because HCN and $H^{14}N^{12}C$ possess a large amplitude motion due to the light hydrogen atom. Mellau and co-workers [10–16] have studied the complete experimental rovibrational eigenenergy system of the [H,^{12}C,^{14}N] molecular system up to 6880 cm^{-1} above the ground state. These papers describe the first full quantum mechanical experimental description of a polyatomic molecule up to highly excited energies (based on the complete eigenvalue list of all compatible observables), the first practically error-free partition function at room temperature for a polyatomic molecule or the first quantitative description for the vibrational onset of the HCN↔HNC isomerization.

The frequency of the bending vibrations of the HCN and HNC isotopologues is low and it fits into the range of high frequency radio telescopes. This has both simplified and accelerated the study of hydrogen cyanide within interstellar space. The Visual and Infrared Mapping Spectrometer (VIMS) was among the twelve instruments aboard the Cassini Orbiter during the Cassini–Huygens mission where the VIMS measured a wave-number range between 11764.71 and 1960.78 cm^{-1} (0.85–5.1 μm) of the Galilean satellites [17].

Due to the astrophysical significance high resolution spectroscopic studies have been carried for several HCN isotopologues such as $H^{13}CN$ [18–21], $H^{13}C^{15}N$ [22], $HC^{15}N$ [20,23] and $D^{13}C^{15}N$ [24]. Ground based millimetric wavelength spectroscopic observations of Titan's atmosphere have substantiated that HCN and a few of its isotopologues such as $HC^{15}N$ are indeed significant constituents of Titan's atmosphere [25–27]. Spectroscopic studies of $HC^{15}N$ are needed to determine the ^{15}N to ^{14}N ratios in planetary atmospheres. In particular, Titan is known to have an unusually high ratio of ^{15}N to ^{14}N, from reasons that are still under investigation.

Only two previous studies [20,23] have been dedicated to the rotation–vibration spectrum of $HC^{15}N$. Rovibrational constants have been determined from absorption spectra for fifty states [23]. Twenty highly excited states have been characterized [20] using emission spectra. In this work, we have studied transitions of the $HC^{15}N$ molecule in the 6050–6500 cm^{-1} spectral region. The ground state constants for $HC^{15}N$ were taken from Refs. [20,23]. Vibrational constants are given for the transitions in combination bands with the following quantum numbers: $0v_20$ to $2v_20$ where v_2 varies from 0 up to 7, $1v_20$ to $3v_20$ where v_2 varies from 0 up to 3, and $0v_21$ to $2v_21$ where v_2 varies from 0 up to 3.

2. Experimental details

The near-infrared (NIR) emission spectrum of $H^{12}C^{15}N$ was measured in the 6050–6500 cm^{-1} range at a resolution of 0.044 cm^{-1}. The measurements were carried out at the Justus-Liebig-University, Giessen, Germany using a Bruker IFS 120 High Resolution Fourier Transform infrared spectrometer and a custom made cell made of quartz. The sample was purchased from Sigma–Aldrich. Using the C_{em} values for the $H^{12}C^{14}N$ and $H^{12}C^{15}N$ isotopologues for several sub-bands reported in Ref. [10] and in the analysis section below, we have determined their average ratio to be 0.056. This finding suggests that the sample contains about 5.6% $H^{12}C^{14}N$ and 94.4% $H^{12}C^{15}N$. The cell was filled with $HC^{15}N$ and heated to 1400 K. The experimental setup is described in detail in Refs. [10,14]. A diagram of the experimental setup is given in Fig. 1. The main components are: the heatable cell, an adjustable iris for limiting the radiative field of view of the infrared beam, an evacuated chamber for transfer optics, the high resolution Fourier Transform infrared (FTIR) spectrometer (not shown in the diagram), and a HeNe laser source. The one meter long emission cell was made of quartz, and had a 5 cm inner diameter. The ends were fitted with CaF_2 windows sealed with Viton O-rings and held at room temperature by water-cooled collars. An electrically heated commercial furnace (RoK/A 6/60, Heraeus, Hanau, Germany) enclosed the central part of the cell yielding a heated region of 60 cm in length at up to 1450 K.

A HeNe laser with an expanded beam is installed at the rear end of the cell tube for the precise alignment of the path for the emission light. In this way the combination of a spherical and a plane mirror in the transfer optics chamber can be carefully adjusted to image the emission perfectly on the entrance aperture through the entrance port and to align the input beam along the optical axis of the interferometer. A mirror was used as the focusing optical element. We believe that CaF_2 lenses used often for emission experiments are not suitable for FT-IR infrared experiments. The vacuum chamber is supported with feather/ spring insulators in order to protect the optics against vibrations in the laboratory.

Once the cell was at the required temperature, it was filled with the $HC^{15}N$ sample gas. Some of the black body background radiation of the hot cell is always recorded together with the sample emission, thus it was necessary to record an emission spectrum of the empty cell and subtract this background spectrum from the sample spectrum, to improve the sample emission spectrum baseline.

On the other hand, this unwanted blackbody radiation increases the overall noise in the spectrum. To minimize this effect two narrow bandpass filters have been used in order to achieve a high signal-to-noise ratio up to 5000:1 for the strongest lines. Two spectra were recorded in the 5998–6401 cm^{-1} and 6298–6649 cm^{-1} range and merged together prior to the spectroscopic analysis. The spectra were recorded at 10 and 11 mbar, respectively. Higher pressures were not used to reduce the effects of pressure broadening and pressure shifts. For each spectrum 820 scans were averaged together to enhance the signal to noise. The full width at half maximum (FWHM) was estimated using the Doppler line shape function to be 0.06 cm^{-1} at a temperature of 1423 K and at line positions of 6275 cm^{-1}, hereby being wider than the 0.044 cm^{-1} resolution. The wavenumber scale has been calibrated using to $2v_20$ HCN overtone transitions [10] present in the spectra as impurity.

3. Spectroscopic analysis and results

The first step in the analysis was to perform the wavelength calibration of the spectra. We performed an internal calibration with respect to the line positions of HCN present in our spectra as a contaminant. Line positions for HCN transitions in the 00^00–20^00, 01^10–21^10 and 02^00–22^00 bands taken from Ref. [10] were used to obtain multiplicative factors for the wavenumber scales of the two spectra. For isolated $HC^{15}N$ lines, the absolute accuracy in our measured line center positions is about ±0.00005 cm^{-1} or better.

To be able to use the intensity information in the assignment procedure it is necessary to calibrate the intensity axis due to the frequency dependence of the overall spectrometer sensitivity. In

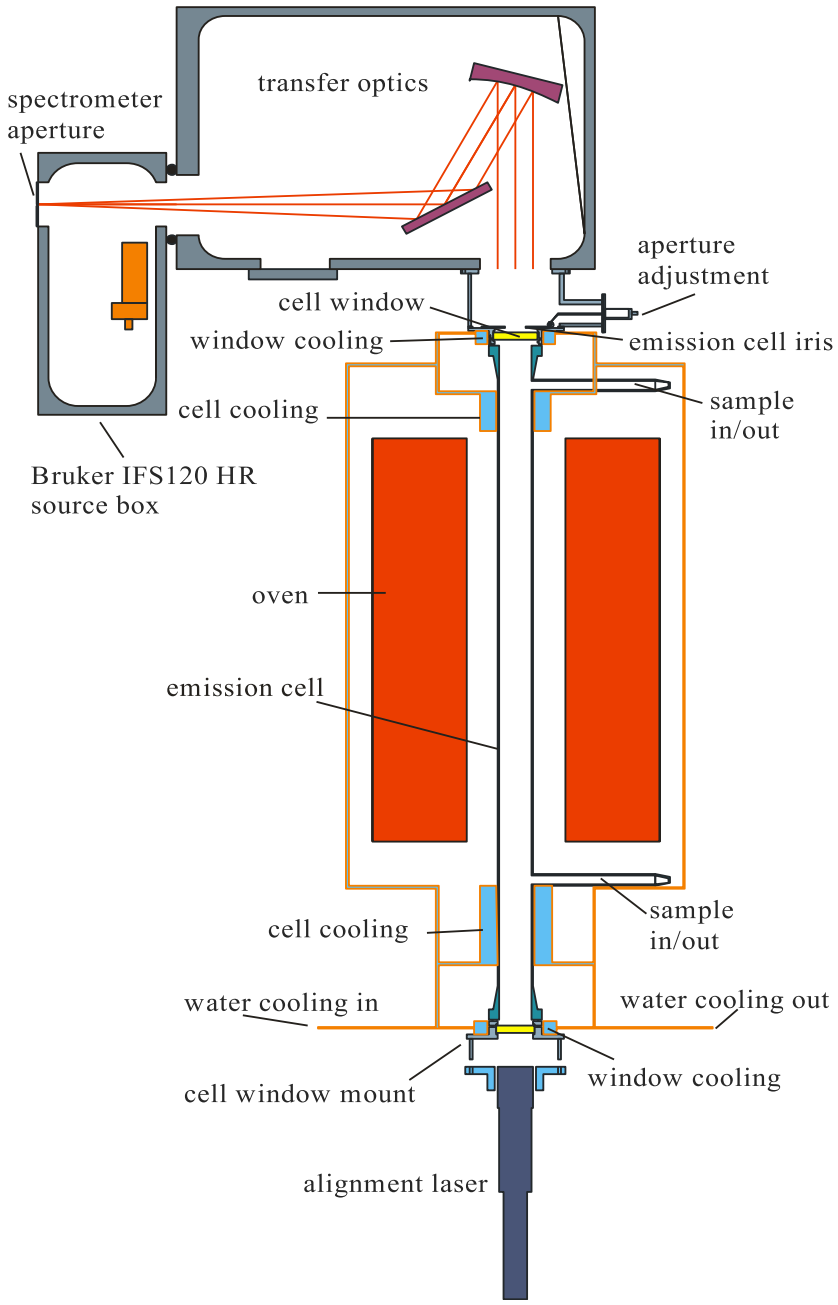

Fig. 1. Schematic diagram of the emission experiment.

a first step the overall intensity of the two spectra has been adjusted until the peaks in the overlapping range had the same intensity. In a second step, we compared the measured and calculated intensities of all isolated transitions for some medium, strong bands and determined an averaged curve for ratios of intensities vs. wavenumber.

The data analysis has been performed using the SyMath software package [8,14], developed by one of the co-authors (G. Mellau). The SyMath package contains three main spectroscopic analysis modules, namely: Molecule, Band Search, and Spectrum Fit. The lineshape analysis feature of the Spectrum Fit module [10] allowed us to accurately identify the peak positions for overlapping transitions. The Molecule program adds an analytical matrix mechanics module to the system. It allows the prediction and analysis of molecular eigenenergies and transitions of any quantum system. The quantum system (in our case the HCN molecule) is described by the user through the analytical formulas entered in special entry fields. In our case it was necessary to define for example the quantum numbers used to label the eigenenergies, the selection rules or the analytical formulas of the matrix elements with the mathematical rules describing the position of nonzero matrix elements. Based on this analytical information about the molecular Hamiltonian (all information is entered as an input by the user in predefined entry fields) the program generates a set of matrixes and calculates where the molecular transitions should be. The most complex part of the SyMath is a computer program manipulating analytical expression which allows that the parameters defined in the analytical formulas defined for the nonzero matrix elements can be adjusted to match the measured transition wavenumbers.

The Band Search program links the user defined lineshape parameters (spectral line position, intensity, line width, etc.) for

each peak saved in the SpectrumFit database to the molecular levels and transition wavenumbers. This system connects the eigenenergies and transitions in a dynamic way to the transitions detected through the lineshape deconvolution procedure. Besides being a general analytical link system, the program implements a semi-automatic spectrum analysis system for a sequential "*band to band*" analysis of molecular spectra. The user can make changes in the lineshape analysis during the assignment of the bands (and thus change the line positions and intensities of the "*peaklist*" used for analysis) of the spectrum according to the additional knowledge that one gains during the fit of the band peaks. The program makes it possible to mark the already assigned peaks of the spectrum helping thus very much in the assignment of very weak bands of dense spectra. The program allows the analysis of strongly overlapping spectra. Hence, the spectroscopic parameters determined are much more precise as if they were determined using just a typical peaklist. An overview of the spectrum of $H^{12}C^{15}N$ is given in panel (A) of Fig. 2. The high density of states can be noticed from the figure. In the lower panel we show a sample of transitions assigned with SyMath.

Once we had a set of assignments the next step was to determine the sub-band origin and the state-specific energy expansion coefficients. The positions of the observed spectral lines, υ_{obs}, were fitted using nonlinear least-squares to the expression:

$$\upsilon_{obs} = T(v,l,J)' - T(v,l,J)'' \tag{1}$$

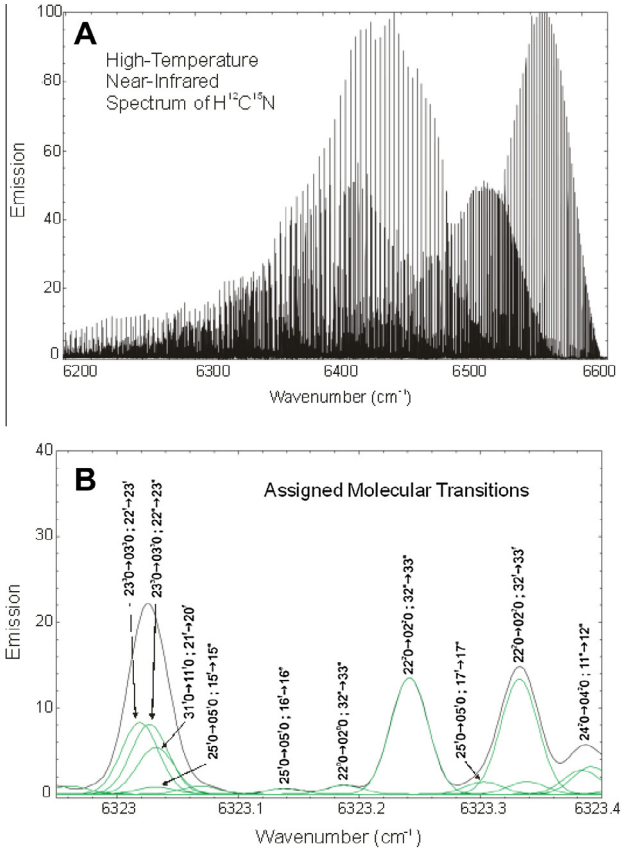

Fig. 2. (A) Overview of the $HC^{15}N$ emission spectra. (B) Sample of transitions assigned using Symath. Note that the dark blue line represents the observed intensity profiles, and the light blue corresponds to the individual transitions. (For interpretation of the references to color in this figure legend, the reader is referred to the web version of this article.)

Here $T(v, l, J)'$ and $T(v, l, J)''$ refer to the upper and lower states, and are given by the appropriate eigenvalues obtained from the matrix of size $(v_2 + 1) \times (v_2 + 1)$ that has as diagonal matrix elements:

$$\begin{aligned} &< v_1, v_2, v_3, l, J|\mathbf{H}/hc|v_1, v_2, v_3, l, J >= T(v,l,J) \\ &= G_v(v,l) + F(v,l,J) \end{aligned} \tag{2}$$

In Eq. (2) the term $F(v, l, J)$ is the unperturbed rotational term value, given by

$$\begin{aligned} F(v,l,J) = B_v[J(J+1) - l^2] - D_v[J(J+1) - l^2]^2 \\ + H_v[J(J+1) - l^2]^3 \end{aligned} \tag{3}$$

and $G_v(v, l)$ is the unperturbed vibrational term value.

To account for the *l*-doubling effects, the off-diagonal matrix elements are

$$\begin{aligned} &< v_1, v_2, v_3, l, J|\mathbf{H}/hc|v_1, v_2, v_3, l \pm 2, J > \\ &= \frac{1}{4}[q_v - q_{vJ}J(J+1) + q_{vJJ}J^2(J+1)^2 + q_l(l \pm 1)^2] \\ &\times \{(v_2 \mp l)(v_2 \pm l + 2)[J(J+1) - l(l \pm 1)] \times [J(J+1) - (l \pm 1)(l \pm 2)\}^{1/2} \end{aligned} \tag{4}$$

and

$$\begin{aligned} &< v_1, v_2, v_3, l, J|\mathbf{H}/hc|v_1, v_2, v_3, l \pm 4, J >= (\rho_v/16)\{(v_2 \mp l)(v_2 \pm l + 2) \\ &(v_2 \mp l - 2) \times (v_2 \pm l + 4)[J(J+1) - l(l \pm 1)][J(J+1) \\ &-(l \pm 1)(l \pm 2)][J(J+1) - (l \pm 2)(l \pm 3)] \times [J(J+1) - (l \pm 3)(l \pm 4)]\}^{1/2} \end{aligned} \tag{5}$$

The q_l term in Eq. [4] is equivalent to the q_t^k term described by Watson [28]. We have determined the rotational constants and *l*-doubling constants for over 1400 transitions. Over 800 transitions were observed for the first time. The new rovibrational constants for $H^{12}C^{15}N$ corrected for *l*-type resonances are listed in Table 1. Table 2 contains the *l*-type resonance constants.

3.1. Perturbations and vibrational coupling

Several assigned sub-bands showed the Coriolis spectral signature of significant shifts in the expected line positions, complementary to those observed for the corresponding interacting sub-bands. Four Coriolis interactions have been observed for the first time. The states involved, position, and interaction constants are given in Table 3. As an initial approach towards quantifying the observed Coriolis coupling, we have modeled each resonance as a simple two level interaction with a *J*-independent Coriolis constant, W_v. We have explored the possibility of determining the *J*-dependent constant, W_{vJ}, but were unable to measure it accurately. The upper and lower interacting energy levels are symmetrically pushed apart with shifts, $\delta(J)$ given by the expression

$$\pm\delta(J) = \pm\frac{1}{2}[\Delta E(J) - \Delta E_o(J)] \tag{6}$$

where $\Delta E(J)$ and $\Delta E_o(J)$ are the separations between perturbed and unperturbed energy levels presented in Table 3 for each pair of states affected by Coriolis interactions.

In the two dimensional secular determinant approach, the perturbed and unperturbed energy levels are related as:

$$\Delta E(J)^2 = \Delta E_o(J)^2 + 4H_{Cor}(J)^2 \tag{7}$$

Depending on the type of Coriolis interaction, the off-diagonal Coriolis matrix element has one of the following two expressions:

Table 1
Rovibrational constants in cm^{-1} for $H^{12}C^{15}N$ corrected for *l*-type resonances.

v_1	v_2	l	v_3	G_{vz} (cm^{-1})	B_v (cm^{-1})	$D_v \times 10^{-6}$ (cm^{-1})	$H_v \times 10^{-12}$ (cm^{-1})	J_{max}
2	0	0	0	6516.50748(8)	1.41494359(17)	2.70048(8)	3.197(9)	72
2	1	1	0	7190.21665(3)	1.41875867(10)	2.77183(7)	3.990(13)	65
2	2	0	0	7848.43134(8)	1.42307649(38)	2.85963(31)	6.055(68)	63
2	2	2	0	7869.06451(5)	1.42226589(23)	2.83512(20)	4.289(44)	61
2	3	1	0	8511.85833(6)	1.42709670(29)	2.92072(30)	7.112(81)	57
2	3	3	0	8553.13596(7)	1.42543890(31)	2.90292(31)	3.549(81)	57
2	4	0	0	9159.86904(15)	1.43164899(82)	2.99747(91)	7.956(269)	51
2	4	2	0	9180.55539(11)	1.43079850(54)	2.98454(57)	6.314(166)	54
2	4	4	0	9242.50934(12)	1.42826038(57)	2.96522(62)	3.249(188)	51
2	5	1	0	9813.13018(28)	1.43592149(153)	3.09374(196)	20.875(641)	55
2	5	3	0	9854.57790(24)	1.43415797(129)	3.04486(161)	2.690(510)	55
2	5	5	0	9937.25985(23)	1.43069291(119)	3.01481(141)	−0.295(448)	55
2	0	0	1	8551.18370(5)	1.40568644(23)	2.71378(18)	4.400(36)	68
2	1	1	1	9222.25284(10)	1.40940465(41)	2.78692(39)	5.1101(99)	60
3	0	0	0	9621.74097(14)	1.40434378(45)	2.68242(33)	4.331(65)	60
2	2	0	1	9878.06601(43)	1.41360467(247)	2.86390(298)	8.114(948)	61
2	2	2	1	9898.48115(29)	1.41281308(150)	2.86001(175)	5.855(549)	61
2	6	0	0	10450.87639(42)	1.44069841(212)	3.11707(143)	10.066	45
2	6	2	0	10471.67539(31)	1.43984272(147)	3.13770(111)	9.094	45
2	6	4	0	10533.97336(24)	1.43715507(104)	3.11481(82)	6.18(363)	45
2	6	6	0	10637.45123(22)	1.43272887(89)	3.07568(63)	1.32(240)	45
2	7	1	0	11093.78964(80)	1.44524602(504)	3.20262(577)	11.205	41
2	7	3	0	11135.52462(69)	1.44342872(417)	3.20125(508)	9.261	41
2	7	5	0	11218.79053(65)	1.43972985(349)	3.15700(367)	5.373	41
2	7	7	0	11343.15177(66)	1.43430802(339)	3.11595(346)	−0.459	41
3	2	0	0	10914.27826(21)	1.41289679(167)	2.85481(272)	11.380(1140)	55
3	2	2	0	10934.46094(16)	1.41209207(117)	2.81857(200)	2.537(889)	55
3	1	1	0	10275.64401(13)	1.40837063(54)	2.75731(52)	5.048(130)	57
3	3	1	0	11557.86792(32)	1.41714186(215)	2.94624(362)	7.190(1620)	55
3	3	3	0	11598.23231(24)	1.41549713(178)	2.90373(292)	0.924(1285)	55
2	3	1	1	10539.08426(38)	1.41753312(223)	2.94659(336)	8.48(142)	45
2	3	3	1	10579.96005(31)	1.41586216(230)	2.91152(401)	−2.50(190)	45

Table 2
Constants for *l*-type resonance energy terms of $H^{12}C^{15}N$ given in cm^{-1}.

v_1	v_2	l	v_3	$q_v \times 10^{-3}$ (cm^{-1}) (45)	$q_{vJ} \times 10^{-8}$ (cm^{-1}) (23)	$q_{vJJ} \times 10^{-12}$ (cm^{-1}) (2)	$\rho_v \times 10^{-8}$ (cm^{-1}) (34)	$q_{lv} \times 10^{-4}$ (cm^{-1})
2	1	1	1	7.28393(14)	9.211(18)	1.59(2)	–	–
2	2	2	1	7.39729(26)	9.820(21)	1.98(4)	–	–
2	3	3	0	7.53611(17)	10.729(19)	2.97(5)	−2.0767(13)	0.0854
2	4	4	0	7.66014(17)	10.819(10)	1.528(0)	−2.0452(55)	0.0854
3	2	2	0	7.47682(170)	10.274(274)	4.00(105)	−0.95	0.0854
2	1	1	0	7.28410(13)	9.230(12)	1.637(2)	−1.7435(0)	0.0828
2	2	2	0	7.39730(26)	9.821(21)	1.985(4)	−0.9520(0)	0.0854
2	5	5	0	7.79933(49)	12.546(68)	5.942(22)	−2.2811(49)	
3	1	1	0	7.35566(66)	10.315(79)	4.092(21)	0.00	0.0828
3	3	3	0	7.62235(62)	9.534(59)	–	−1.7429(240)	0.0854
2	3	3	1	7.63299(60)	10.854(55)	–	−2.1048(222)	0.0854
2	6	6	0	7.92571(43)	11.741(35)	–	−2.1964(9)	
2	7	7	0	8.09242(125)	15.122(156)	–	−2.6220(503)	0.0854

$$< v_1, v_2, v_3, l, J|\mathbf{H}_{Cor}/hc|v_1, v_2+3, v_3-1, l\pm 1, J > = [W_v + W_{vJ}J(J+1)][J(J+1) - l(l\pm 1)]^{1/2} \quad (8)$$

$$< v_1, v_2, v_3, l, J|\mathbf{H}_{Cor}/hc|v_1, v_2+3, v_3-1, l\pm 3, J > = [W_v + W_{vJ}J(J+1)][J(J+1) - l(l\pm 3)]^{1/2} \quad (9)$$

In two of the four new Coriolis resonances observed, a single perturbation constant, W_v, could be determined for the coupling between a given pair of states. In Table 3 we have given the effective interaction constant at the J value for two of the four energy crossing points.

3.2. Intensity analysis

The expression for intensities of emission lines in $HC^{15}N$ is [10]:

$$S(v,l,J) = f_1 C_{em}[100c(T'_z - T''_z)^3 \times S_v S_r \frac{273.15L}{3hT} e^{-\frac{100hcT'_z}{kT}} \quad (10)$$

where, $C_{em} = \frac{f_2 \times \mu^2 AF}{Q_r Q_v}$ is the intensity parameter which is determined for each band intensity using SyMath, and is proportional to the square of the transition dipole moment. f_1 is the scaling factor of this intensity formula and it limits the magnitude of the intensity parameter for each band between 1 and 100. S_v is a dimensionless vibrational intensity factor and S_r is the dimensionless Hönl–London rotational intensity factor. T'_z represents the rovibrational term value for the upper and T''_z for the lower state. T is the temperature of the gaseous sample in Kelvin, L is the Loschmidt number, k is the Boltzmann constant and c is the speed of light.

In the expression for C_{em}, A is the isotopic abundance factor, F is the Hermann–Wallis factor, Q_v and Q_r are the dimensionless vibrational and rotational partition functions at the temperature of

Table 3
New Coriolis Interactions Found for $H^{12}C^{15}N$.

States involved	J at Avoided crossing	Unperturbed energy separation (cm^{-1})	Perturbed energy separation (cm^{-1})	Uppermost level at crossing	Shift due to interaction (cm^{-1})	Interaction constant W_v (cm^{-1})
$22^{0e}1$–$25^{3e}0$	37	0.122	0.1653	$25^{3e}0$	0.0216	0.00148
$03^{3e}1$–$06^{2e}0$	20	0.300	–	$03^{3e}1$	–	–
$03^{3f}1$–$06^{2f}0$	25	0.400	0.46174	06^2 0	0.03087	0.00452
$23^{1e}1$–$26^{4e}0$	29	0.311	–	$23^{1e}1$	–	–

Table 4
The list of $\Delta l = 0H^{12}C^{15}N$ subbands of the $0v_2^l0 \rightarrow 2v_2^l0$ where v_2 varies from 0 up to 7, $1v_2^l0 \rightarrow 3v_2^l0$ where v_2 varies from 0 up to 3, and $0v_2^l1 \rightarrow 2v_2^l1$ where v_2 varies from 0 up to 3 in this work.

Transition	Type	J_{max}	C_{em} (a.u.) [a]	S_v [b]
$00^00 \rightarrow 20^00$	PR	72	26.51	1
$01^10 \rightarrow 21^10$	PR	65	22.30	1
$02^00 \rightarrow 22^00$	PR	63	21.567	1
$02^20 \rightarrow 22^20$	PR	61	21.567	1
$23^10 \rightarrow 03^10$	PR	57	20.10	1
$23^30 \rightarrow 03^30$	PR	57	20.10	1
$04^00 \rightarrow 24^00$	PR	51	18.00	1
$04^20 \rightarrow 24^20$	PR	54	18.00	1
$04^40 \rightarrow 24^40$	PR	51	18.00	1
$05^10 \rightarrow 25^10$	PR	55	17.35	1
$05^30 \rightarrow 25^30$	PR	55	17.35	1
$05^50 \rightarrow 25^50$	PR	55	17.35	1
$06^00 \rightarrow 26^00$	PR	45	15.00	1
$06^20 \rightarrow 26^20$	PR	45	15.00	1
$06^40 \rightarrow 26^40$	PR	45	15.00	1
$06^60 \rightarrow 26^60$	PR	45	15.00	1
$07^10 \rightarrow 27^10$	PR	41	15.00	1
$07^30 \rightarrow 27^30$	PR	41	15.00	1
$07^50 \rightarrow 27^50$	PR	41	15.00	1
$07^70 \rightarrow 27^70$	PR	41	15.00	1
$00^01 \rightarrow 20^01$	PR	68	24.22	1
$01^11 \rightarrow 21^11$	PR	60	20.00	1
$02^01 \rightarrow 22^01$	PR	61	18.40	1
$02^21 \rightarrow 22^21$	PR	61	18.40	1
$03^11 \rightarrow 23^11$	PR	45	16.40	1
$03^31 \rightarrow 23^31$	PR	45	16.40	1
$10^00 \rightarrow 30^00$	PR	60	22.18	3
$11^10 \rightarrow 31^10$	PR	57	20.50	3
$12^00 \rightarrow 32^00$	PR	55	19.80	3
$12^20 \rightarrow 32^20$	PR	55	19.80	3
$13^10 \rightarrow 33^10$	PR	55	16.80	3
$13^30 \rightarrow 33^30$	PR	55	16.80	3

[a] C_{em} is the observed intensity factor proportional to the square of the transition dipole moment.
[b] S_v is the calculated vibrational factor for hot band transitions.

measurement and the absolute value of μ^2 is the square of the vibrational transition dipole matrix element.

The intensity parameters determined for each band are presented in Table 4. The results were determined by comparing the simulated and measured spectrum and fine tuning the adjustable parameters. As reported in Ref. [10], without performing an intensity calibration we were able to model the unknown bands, search for individual lines in the spectrum and ultimately obtain a good agreement between the measured and calculated line intensities.

4. Conclusion

We present extended assignments in the near-infrared emission spectrum of $HC^{15}N$ needed to explore the ladder of bending vibrational states up to very high term values. Several levels containing more than one quanta of bending vibration were observed for the first time. High rotational levels up to $J = 72$ were observed as well as vibrational levels up to 7. Previously published assignments have been extended to high J values. The spectra were analyzed with the spectroscopic analysis software package Symath running using Mathematica as a platform. The lineshape analysis feature of the software allowed us to uniquely identify overlapping transitions. The high accuracy rovibrational levels for $HC^{15}N$ reported in our study will enable the modeling of this molecule's energy structure needed in many practical applications.

Acknowledgments

A. Predoi-Cross acknowledges the support she received from the National Sciences and Engineering Research Council of Canada, University of Lethbridge Research Fund and the Summer Temporary Employment Program of the Government of Canada.

Appendix A. Supplementary material

Supplementary data associated with this article can be found, in the online version, at http://dx.doi.org/10.1016/j.jms.2013.10.002.

References

[1] M. Levy, S.L. Miller, K. Brinton, J.L. Bada, Icarus 135 (2000) 609–613.
[2] A.G. Maki, J. Phys. Chem. Rex Data 3 (1974) 221–244.
[3] D.E. McElcheran, M.H.J. Wijnen, E.W.R. Steacie, Can. J. Chem. 36 (1958) 321–329.
[4] P.B. Asycough, H. Drawe, P. Kohler, Radiat. Res. 33 (1968) 263–273.
[5] R. Moreno, A. Marten, H.E. Matthews, Y. Biraud, P&SS 51 (2003) 591–611.
[6] L. Delaye, A. Lazcano, Phys. Life Rev. 2 (2005) 47–64.
[7] J. Oro, T. Mills, A. Lazcano, Orig. Life 21 (1992) 267–277.
[8] T.G. Custer, S. Kato, R. Fall, V.M. Bierbaum, Int. J. Mass Spectromet. 223 (2003) 427–446.
[9] C.P. Rinsland, A. Goldman, R. Zander, E. Mahieu, J. Quant. Spectrosc. Radiat. Transfer 69 (2001) 3–8.
[10] G.Ch. Mellau, B.P. Winnewisser, M. Winnewisser, J. Mol. Spectrosc. 249 (2008) 23–42.
[11] G.Ch. Mellau, J. Mol. Spectrosc. 264 (2010) 2–9.
[12] G.Ch. Mellau, J. Mol. Spectrosc. 269 (2011) 12–20.
[13] G.Ch. Mellau, J. Mol. Spectrosc. 269 (2011) 77–85.
[14] G.Ch. Mellau, J. Chem. Phys. 133 (2010) 164303.
[15] G.Ch. Mellau, J. Chem. Phys. 134 (2011) 194302.
[16] G.Ch. Mellau, J. Chem. Phys. 134 (2011) 234303.
[17] T.B. McCord, A. Coradini, C.A. Hibbitts, F. Capaccioni, G.B. Hansen, G. Filacchione, R.N. Clark, P. Cerroni, R.H. Brown, K.H. Baines, G. Bellucci, J.-P. Bibring, B.J. Buratti, E. Bussoletti, M. Combes, D.P. Cruikshank, P. Drossart, V. Formisano, R. Jaumann, Y. Langevin, D.L. Matson, R.M. Nelson, P.D. Nicholson, B. Sicardy, C. Sotin, Icarus 172 (2004) 104–126.
[18] R.E. Kagarise, H.D. Rix, D.H. Rank, Some molecular constant of $H^{13}CN$ L, Chem. Phys. 20 (1952) 1437–1438.
[19] D. Romanini, K.K. Lehmann, J. Chem. Phys. 102 (1995) 633–642.
[20] A.G. Maki, G.Ch. Mellau, S. Klee, M. Winnewisser, W. Quapp, J. Mol. Spectrosc. 202 (2000) 67–82.
[21] J.P. Hofmann, B. Eifert, G.Ch. Mellau, J. Mol. Spectrosc. 262 (2010) 75–81.
[22] W. Quapp, V. Melnikov, G.Ch. Mellau, J. Mol. Spectrosc. 211 (2002) 189–197.
[23] A.G. Maki, Wolfgang Quapp, Stefan Klee, Georg Ch. Mellau, Sieghard Albert, J. Mol. Spectrosc. 180 (1996) 323–336.
[24] W. Quapp, M. Hirsch, G.C. Mellau, S. Klee, M. Winnewisser, A. Maki, J. Mol. Spectrosc. 195 (1999) 284–298.
[25] H. Lammer, W. Stumptner, G.J. Molina-Cuberos, S.J. Bauer, T. Owen, P&SS 48 (2000) 529–543.
[26] T. Penz, H. Lammer, Yu.N. Kulikov, H.K. Biernat, Adv. Space Res. 36 (2005) 241–250.
[27] A. Marten, T. Hidayat, Y. Biraud, R. Moreno, Icarus 158 (2002) 532–544.
[28] J.K.G. Watson, J. Mol. Spectrosc. 39 (1983) 364–379.